Near-field optical microscopy and spectroscopy of one-dimensional metallic photonic crystal slabs

S. Linden
Institut für Nanotechnologie, Forschungszentrum Karlsruhe in der Helmholtz-Gemeinschaft, D-76021 Karlsruhe, Germany

N. Rau, U. Neuberth, A. Naber, and M. Wegener
Institut für Angewandte Physik, Universität Karlsruhe (TH), D-76131 Karlsruhe, Germany

S. Pereira
Institut für Theorie der Kondensierten Materie, Universität Karlsruhe (TH), D-76131 Karlsruhe, Germany and Centre d'optique, photonique et laser, Université Laval, Sainte-Foy, Que G1K 7P4, Canada

K. Busch
Institut für Theorie der Kondensierten Materie, Universität Karlsruhe (TH), D-76131 Karlsruhe, Germany and Department of Physics and College of Optics & Photonics: CREOL & FPCE, University of Central Florida, Orlando, Florida 32816, USA

A. Christ and J. Kuhl
Max-Planck-Institut für Festkörperforschung, D-70569 Stuttgart, Germany
(Received 23 December 2004; published 30 June 2005)

We use scanning near-field optical microscopy and spectroscopy to investigate the near field of one-dimensional periodic arrays of gold nanowires on top of a slab waveguide. The Bragg resonance of these one-dimensional metallic photonic crystal slabs can coincide with the particle-plasmon resonance of the metal nanowires, giving rise to an avoided crossing. We find a rich behavior when systematically varying the polarization of the incident light, the lattice constant, and the slab thickness. Numerical simulations of the transverse magnetic component of the near field qualitatively reproduce the experiment, in agreement with the expectation from the Bethe-Bouwkamp theory. Furthermore, these calculations give insight into those electromagnetic field components which cannot easily be measured.

DOI: 10.1103/PhysRevB.71.245119 PACS number(s): 42.70.Qs, 07.79.Fc, 73.20.Mf

I. INTRODUCTION

The optical properties of bulk metals are often well described by the Drude model of free electrons in a crystal. This changes drastically for a metal nanostructure. If the metal dimensions along the electric field vector of the incident light become comparable to the wavelength of light, one obtains a Lorentz oscillator response rather than a Drude response. In the electrostatic limit, this can easily be understood in terms of charges accumulating at the metal surface. These charges induce a depolarization field that can either counteract or enhance the external electric field of the light, depending on the permittivity of the metal, hence depending on the frequency of light. The resulting well-known optical resonance at this transition point is often referred to as the particle-plasmon resonance.[1]

If such metal nanostructures are arranged into a periodic array, a peculiar photonic crystal results. The usual photonic crystals are D-dimensional periodic arrangements ($D=1,2,3$) of some high-index material and air.[2,3] The refractive index of the dielectric can be assumed to be frequency independent. In contrast to this, for a metallic photonic crystal, the particle-plasmon resonance frequency can be close or identical to the Bragg frequency of the photonic crystal, giving rise to a double-resonance situation. As usual, one anticipates an avoided crossing. Related double-resonance situations have been discussed for excitons coupled to a one-dimensional Bragg mode[4] and for a phonon mode coupled to a two-dimensional photonic crystal.[5,6]

If, for example, metallic nanoparticles are arranged in a two-dimensional array on the surface of some dielectric substrate, with a lattice constant comparable to the relevant wavelength of light, the resulting coupling of the particle-plasmon resonances turns out to be fairly small.[7] If, on the other hand, the coupling is facilitated by a slab waveguide underneath the metal nanoparticles, the propagating electromagnetic mode in the slab gives rise to a very strong coupling. *The presence of a slab waveguide makes these periodic metallic nanostructures distinct from the usual metallic gratings*. This aspect, combined with the large oscillator strength of the particle-plasmon resonances, has given rise to measured splittings on the order of 250 meV.[8,9] This has to be compared with splittings of just a few meV seen for one-dimensional exciton Bragg structures.[4]

Two-dimensional metallic photonic crystal slabs were first discussed in Ref. 8. They employed gold nanoparticles. Later,[9] gold nanowires have shown even more pronounced effects. One charming aspect of these one-dimensional photonic crystals made from metal nanowires is that one can control the coupling to the particle-plasmon resonance via the polarization of the incident light. If the electric field vector is oriented perpendicular to the nanowires (TM polarization), a pronounced depolarization field arises, giving rise to a strong optical resonance. In contrast, if the electric field

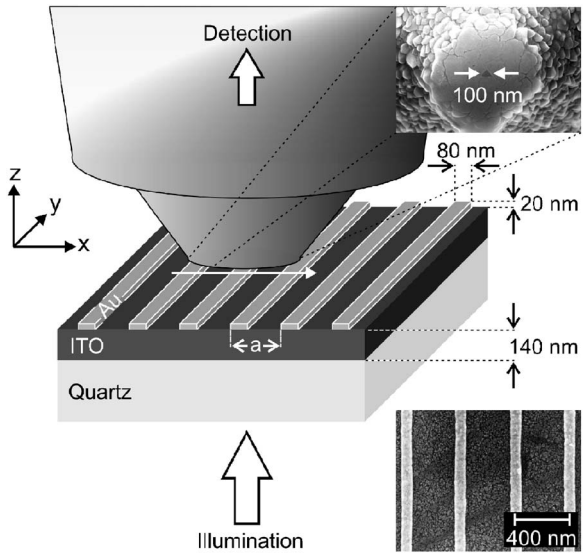

FIG. 1. Scheme of the near-field optical experiment. The electron micrographs of a typical sample and of the aperture probe on the right-hand side are shown on the same scale to allow for a direct comparison.

vector is along the wire axis (TE polarization), the depolarization factor is zero and one rather obtains a Drude type of response. Today, the far-field linear optical properties of such structures are well understood and detailed numerical calculations have been performed.[10] For an intuitive understanding, one is obviously interested in the electromagnetic field distribution in the vicinity of the metal nanostructures—i.e., in the optical near field. It can be viewed as the analog of the electronic wave function in a usual crystal. Corresponding calculations have been presented,[10] but we are not aware of any experimental results. In this paper, we present and discuss corresponding experiments with a scanning near-field optical microscope, used in a transmission mode and combined with a spectrometer.

II. EXPERIMENTS

The one-dimensional metallic photonic crystal slabs in our experiments are fabricated by means of standard electron-beam lithography. These samples consist of a quartz substrate, a dielectric layer [indium tin oxide (ITO)] of thickness $d=140$ nm, and gold nanowires of 80 nm in width and 20 nm in height, periodically arranged with lattice constant a (see insets in Fig. 1). Their normal-incidence far-field transmission spectra are shown in Fig. 2 for the two orthogonal linear polarizations and for different lattice constants a as indicated. The spectra in Fig. 2 indeed reveal the behavior anticipated from our above introductory discussion. If the electric field is polarized along the metal wires [Fig. 2(a)], no coupling to the particle-plasmon resonance results. One transmission dip is seen for each lattice constant, which simply results from the fact that one particular wavelength can be Bragg diffracted into the waveguide mode, leading to reduced transmission in the direction normal to the waveguide.

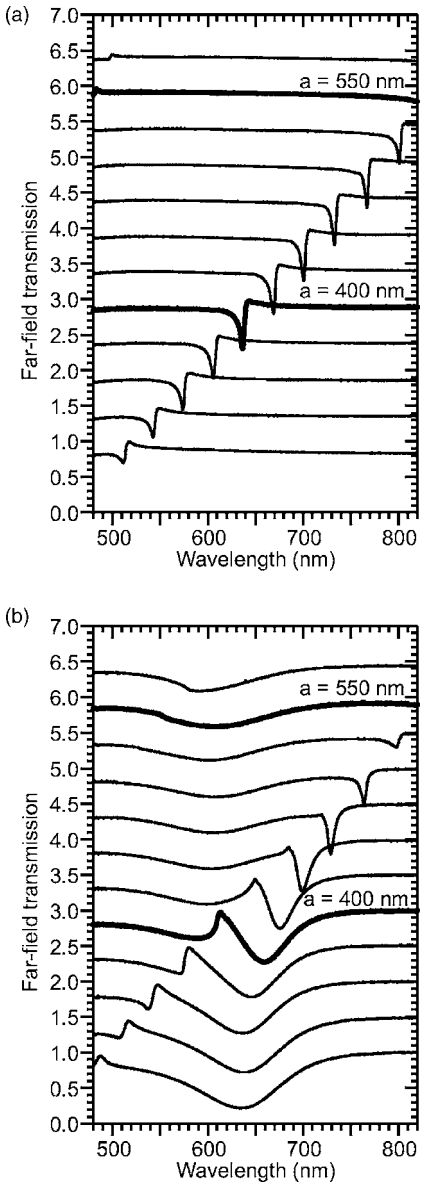

FIG. 2. Normal-incidence, far-field transmission spectra for two orthogonal linear polarizations and for different lattice constants a from 300 nm to 575 nm in steps of 25 nm. The curves for different values of a are shifted for clarity. (a) TE polarization, i.e., incident electric field vector along the metal nanowires, (b) TM polarization, i.e., electric field vector perpendicular to the wires.

The position of the dip simply follows the lattice constant. In contrast, if the electric field vector is perpendicular to the metal wires, strong coupling to the particle-plasmon resonance results. Thus, two transmission dips are seen for all lattice constants in Fig. 2(b). When the Bragg dip meets the particle-plasmon resonance (roughly in the middle of the spectral interval shown), the two do *not* cross but rather exhibit an avoided crossing. We have performed near-field optical experiments on all of these samples. The main physics, however, becomes already clear from considering the two special cases highlighted by thicker lines in Fig. 2: $a=400$ nm is the case of strong intermixing of Bragg and

particle-plasmon resonance, respectively, and $a=550$ nm is an off-resonant case.

In our near-field experiments, we illuminate the structures through the substrate with the white-light spectrum from a 20 W light bulb (see Fig. 1). The light is imaged to a spot of 100 μm in diameter by a lens with a numerical aperture of NA=0.22. Since the intensity of the incident light field is approximately constant over many lattice constants, we can assume that the sample is locally excited by a plane wave. The light in the optical near-field of the structure is collected with an optical aperture probe operated in the constant-gap mode with a distance of a few nanometers. The aperture probes are fabricated by a two-step etching process of an optical glass fiber,[11] followed by a full metallization with aluminum and subsequent "pounding" of the tip on a smooth substrate.[12] We reproducibly get aperture diameters somewhat below 100 nm [see upper right-hand-side (RHS) inset in Fig. 1] as well as large light throughput. All experiments outlined below have been reproduced with several different fiber probes. The collected light is sent into a grating spectrometer connected to a sensitive, liquid-nitrogen-cooled charged-coupled-device camera. Typical spectra shown below are acquired within 10 sec exposure time each. By performing one-dimensional line scans perpendicular to the gold nanowires, we obtain two-dimensional data sets which represent the complete spatiospectral near-field distribution.

We start with a very simple case: The electric field vector is oriented along the metal wires (TE polarization) and no coupling to the particle-plasmon resonance is expected [also see Fig. 2(a)]. Figures 3(a) and 3(b) show the corresponding spatially and spectrally resolved intensity collected in the near field for the lattice constants of $a=550$ nm and $a=400$ nm, respectively. The intensity collected with the near-field probe is normalized with respect to that of the bare ITO waveguide. For both lattice constants, low light intensity results if the aperture probe is positioned behind the metal wires, whereas large intensity is observed between the metal wires. This behavior corresponds to the naive expectation from geometrical optics for an opaque metal. For wavelengths near the maximum in the far-field transmission in Fig. 3(b), we observe bright peaks between the gold nanowires. This is expected from the corresponding standing-wave pattern at the Bragg frequency.

Next, we consider the more interesting orthogonal linear polarization (TM polarization)—i.e., an electric field vector perpendicular to the metal wires. In Fig. 4(a), the Bragg frequency is below the particle-plasmon frequency and we observe the light intensity behind the gold nanowires is enhanced by as much as a factor of 4 for wavelengths longer than the particle-plasmon resonance. In contrast, for shorter wavelengths, the light intensity behind the nanowires is low. This contrast inversion occurs near to the center of the particle-plasmon resonance and is obviously related to the phase variation of a harmonic oscillator near to its resonance. The light intensity between the nanowires is complementary.

A similar behavior is observed in additional experiments on isolated single metal wires (Fig. 5). Comparing Figs. 5(b) and 4(a) for TM polarization yields a similar behavior, comparing Figs. 5(a) and 3(a) for TE polarization as well. Thus, the features visible in Fig. 4(a) are dominated by the independent response from the nanowires, and the lattice constant a plays no important role.

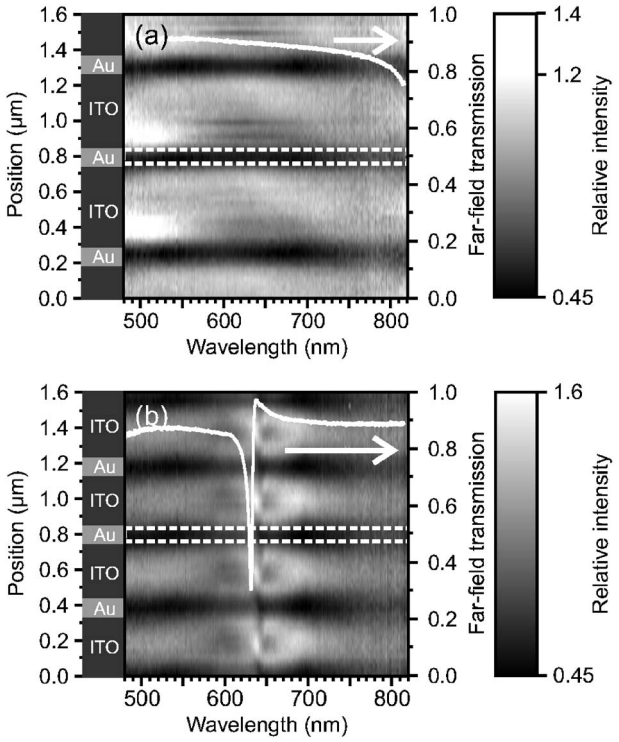

FIG. 3. Grey-scale images of the normalized intensity measured with the near-field aperture probe versus wavelength and tip position. The aperture probe is operated in the constant-gap mode with a distance of a few nanometers. The incident polarization is TE. Lattice constants are (a) $a=550$ nm and (b) 400 nm, respectively. The corresponding far-field transmission spectra are shown by the white curves [compare with Fig. 2(a)]. The position of the gold nanowires is indicated on the LHS as well as by the dotted white lines.

Most interestingly, Fig. 4(b) depicts the measured near-field distribution for the double-resonance condition where the Bragg frequency coincides with the particle-plasmon frequency. For the very-long- and short-wavelength limits, respectively, the behavior in Fig. 4(b) is similar to that in (a). However, in the double-resonance region, a distinct spatial reconfiguration of the optical near-field is observed. Close to the far-field transmission maximum in the center as well as to its RHS, the intensity is redistributed towards the edges of the gold nanowires, giving rise to a doubling of the spatial frequency. The spatial redistribution of the optical near field happens on both sides of the resonance in a wavelength interval of less than 20 nm. Comparison of Figs. 4 and 3, respectively, evidently shows that the coupling to the particle-plasmon resonance is one crucial ingredient for this behavior. To further investigate the underlying mechanism, we have performed additional experiments in which we effectively switch off the waveguide by using much thinner ITO layers with $d=30$ nm. Here, the cutoff frequency of the slab waveguide is shifted towards larger frequencies outside the depicted interval. For this substrate and a period of $a=400$ nm (not shown), the maximum in the far-field trans-

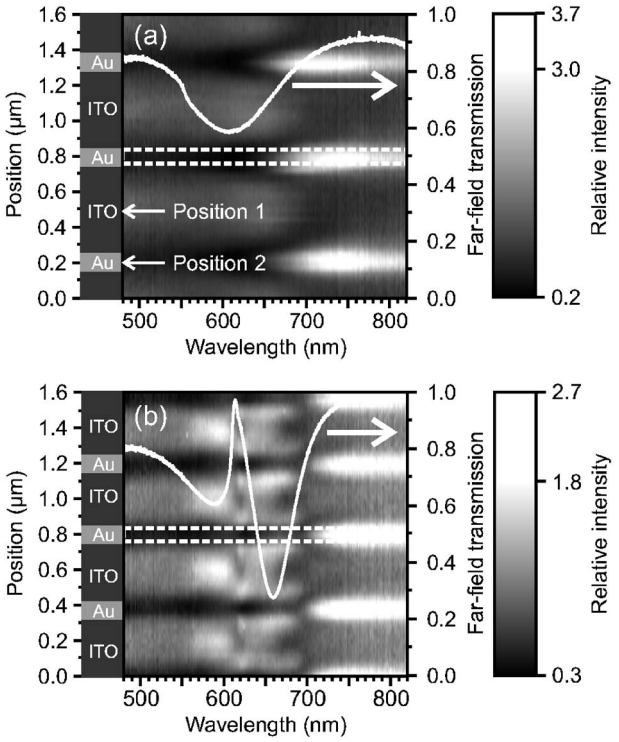

FIG. 4. As Fig. 3, but for TM-polarized light. The two positions discussed in Fig. 6 are marked by arrows.

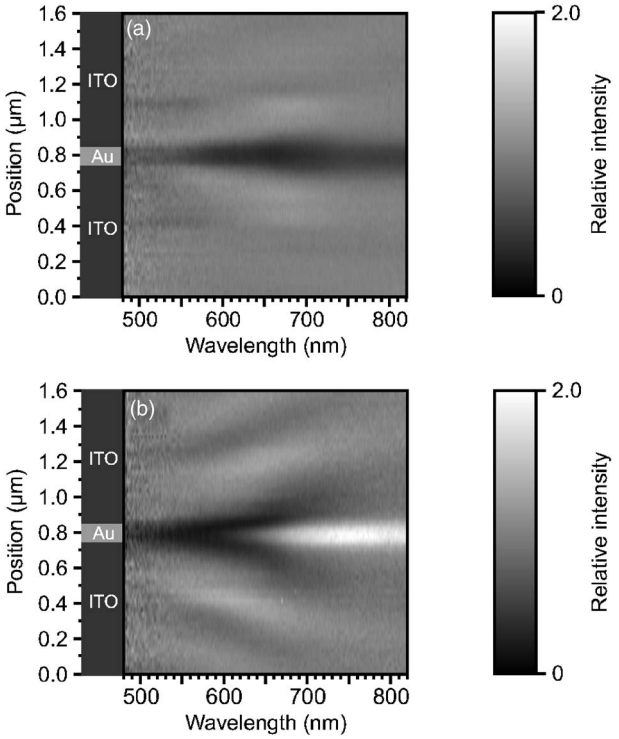

FIG. 5. As in Figs. 3 and 4, but for a *single* gold nanowire rather than a periodic arrangement. (a) TE polarization and (b) TM polarization.

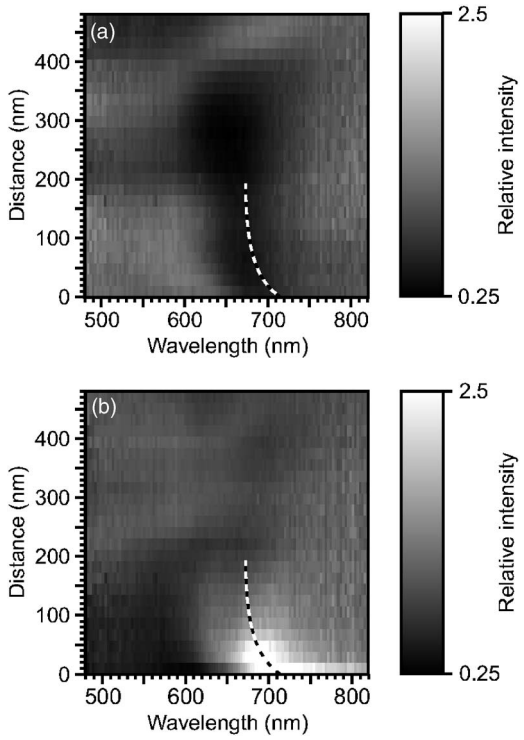

FIG. 6. Variation of the intensity versus tip-sample distance at the two sample positions marked in Fig. 4: (a) position 1: tip is between two gold nanowires, (b) position 2: tip is on top of a gold nanowire. The dashed curves are guides to the eye.

mission as well as the additional features in the near-field data in Fig. 4(b) vanishes and a behavior close to Fig. 4(a) is recovered. These two aspects together unambiguously show that the complex spatial reconfiguration of the optical near field seen in Fig. 4(b) is a direct consequence of the coupling of the plasmon and Bragg resonance.

III. THEORY AND DISCUSSION

As usual, the interpretation of near-field optical data requires some caution.[13] Two issues need to be addressed before comparing our experiments to theoretical calculations: (i) Does the presence of the near-field probe substantially distort the field distribution? (ii) What is it that one actually measures with the near-field aperture probe?

(i) We have performed both additional experiments as well as specific simulations to clarify this point. In the experiments, we position the near-field probe behind a gold stripe and take spectra as a function of the tip-sample separation. This is shown in Fig. 6 for the same sample and configuration as in Fig. 4(a). We find that the spectral features associated with the particle-plasmon resonance do shift by a few tens of nanometers due to the changing dielectric environment.[14] This shift in Fig. 6, however, is still smaller than the width of the particle-plasmon resonance. Furthermore, for a wavelength of, e.g., 700 nm and at tip-sample distances larger than 50 nm in Fig. 6 (see dashed curve), the enhanced intensity behind the gold stripe turns into a reduced intensity, indicating that the field detected by the probe is no

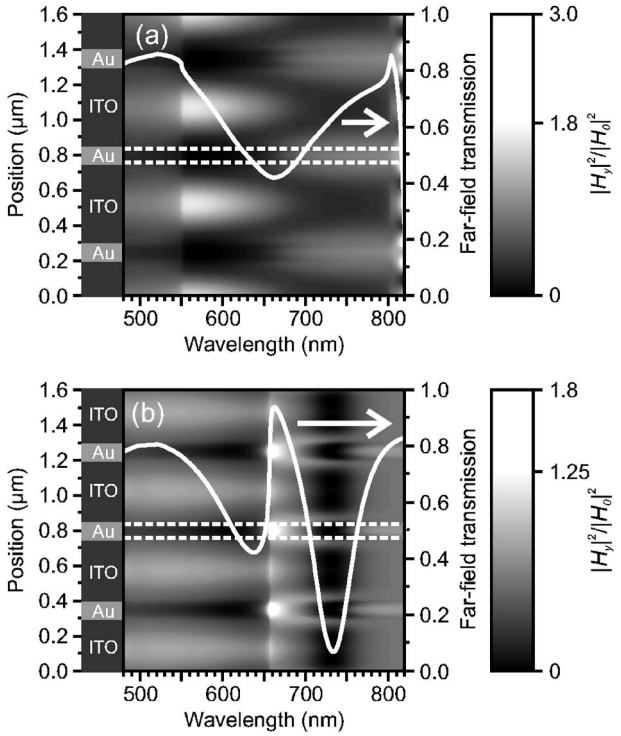

FIG. 7. Calculated field distribution $|H_y|^2$ in a plane 10 nm above the gold nanowires (Fig. 2), versus wavelength and spatial coordinate, presented in the same form as the experiment (Fig. 4). H_0 is the amplitude of the incident magnetic field, and the incident polarization is TM. Lattice constants are (a) $a=550$ nm and (b) 400 nm, respectively.

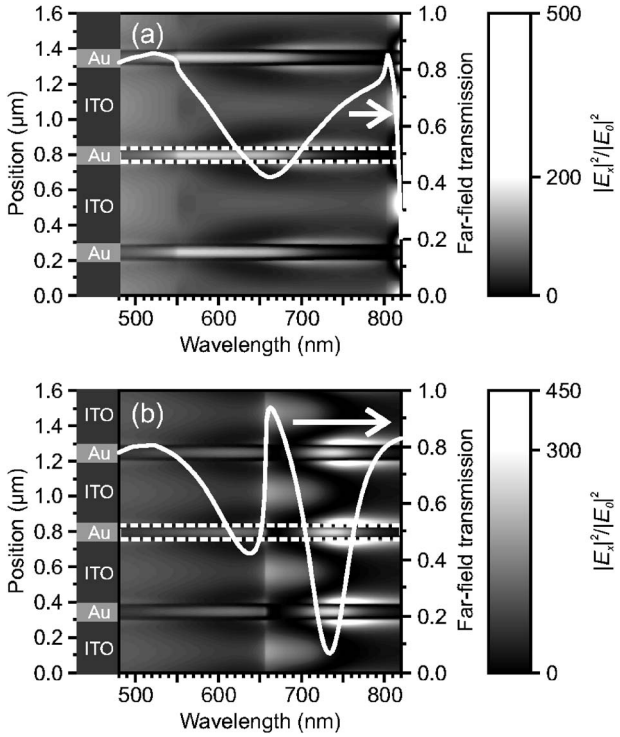

FIG. 8. As in Fig. 7, but for $|E_x|^2$. E_0 is the amplitude of the incident electric field.

longer dominated by the evanescent components. The behavior at large tip-sample distances is dominated by standing-wave effects. The theoretical simulations described below also indicate that the influence of the tip, which can be regarded as a metal half-space to first approximation (see Fig. 2), changes the emphasis of different features in the near-field distribution but keeps the overall qualitative scenario intact. Indeed, the mere fact that the spectral position of the features in the far-field spectra coincides with the features in the near-field data (e.g., Fig. 4) also points in this direction.

(ii) Still, one needs to address what exactly is measured with the aperture probe. Years ago, Bethe considered a subwavelength aperture in an ideal metal film of vanishing thickness. From the corresponding Bethe-Bouwkamp theory[15,16] it is well known that such an aperture mainly collects the transverse component of the magnetic field, H_y, and the longitudinal component of the electric field, E_z, whereas the transverse component of the electric field, E_x, is *not* efficiently coupled to. This is a simple result of the screening of the metal film. Based on these considerations, it is interesting to compare the calculated components H_y and E_z with our *near-field* experiments. In addition, one expects that the features in the optical *far-field* spectra are dominated by the E_x component.

Our theoretical modeling is based on a scattering-matrix formalism[17,18] which allows accurate calculations of transmission properties as well as electric and magnetic field distributions for the above geometry. The parameters are directly taken from the experiment[19] and the linear dielectric function of bulk gold is taken from Ref. 20. Results for the interesting TM polarization are shown in Figs. 7 and 8 for the components H_y and E_x, respectively, in a plane 10 nm above the gold nanowires. The graphical presentation is according to the experiments shown in Figs. 3 and 4. Figure 7 qualitatively resembles the optical near-field observed in the experiment (Fig. 4). Specifically, for the off-resonant case (a), the contrast inverts around the center of the particle-plasmon resonance. This is a consequence of the phase shift of the particle plasmon by π with respect to the driving light field when going through the resonance. In resonance, (b), the short- and long-wavelength limits, respectively, are again similar to (a), whereas close to the far-field transmission peak in the center, intensity maxima occur at the edges of the metal nanowires, leading to a doubling of the spatial frequency as in the experiment [Fig. 4(b)]. In this fashion, the electromagnetic field configuration corresponding to the mixed state "avoids" the metal. While there is a one-to-one correspondence for most features in theory and experiment, the calculated intensity maxima behind the gold nanowires at the spectral position of the far-field transmission peak in Fig. 7(b) have no counterpart in the corresponding experimental data. This might be related to the finite opening angle of the incident light in the experiment.

The behavior of the transverse electric component, E_x, shown in Fig. 8 is different from H_y. This is expected since there is a phase shift between the electric and magnetic fields in the near-field zone of a scattering particle. Note that the contrast in Fig. 8(a) is close to opposite with respect to Fig. 7(a). In particular, it is dark (bright) behind the gold nanowires on the long-wavelength (short-wavelength) end in Fig.

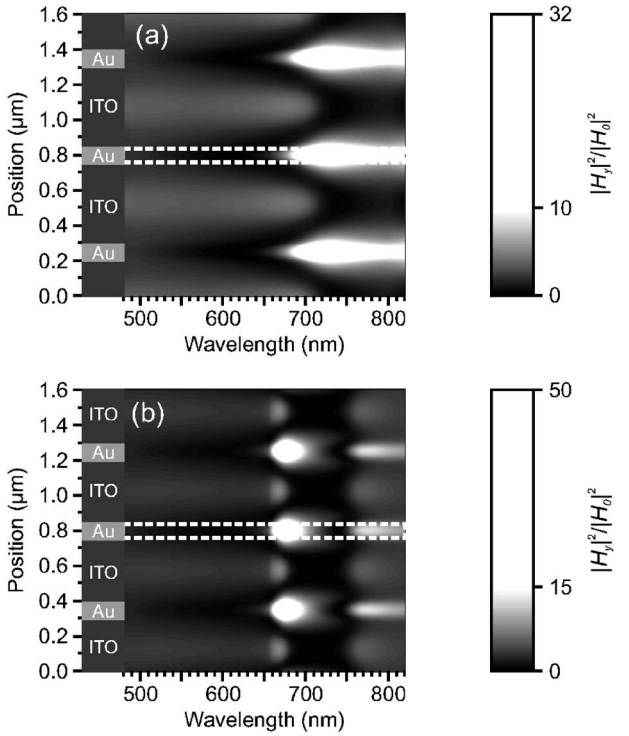

FIG. 9. As in Fig. 7, but with an additional aluminum half-space, separated from the gold nanowires by 20 nm. This half-space roughly mimics the presence of the aperture probe in the experiments (see Fig. 1).

8(a), which is opposite to Fig. 7(a). Moreover, the behavior for the resonant case [compare Figs. 7(b) and 8(b)] is also quite different. The E_z component for both periods a is completely dominated by maxima at the edges of the metal nanowires (not shown). This is a result of the dipole character of the excited particle plasmon. The other components E_y, H_x, and H_z are strictly zero by symmetry. We have performed additional calculations for all of the discussed cases by adding a metal (aluminum) half-space at a distance of 20 nm from the gold nanowires. This roughly mimics the presence of the near-field optical aperture probe (see Fig. 1). While the magnitude of field enhancement changes and some shift of the resonance features does occur, the overall qualitative scenario remains similar. This can be seen from a comparison of Figs. 9 and 7, both depicting the H_y component, and supports our above interpretation based on independent experimental findings. Finally—again in agreement with experiment—the described features disappear if the incident polarization is switched from TM to TE (not shown).

IV. SUMMARY

In conclusion, taking advantage of the combined capability of optical near-field *spectroscopy and microscopy*, we have mapped out the optical near-field distribution of one-dimensional metallic photonic crystal slabs. In the double-resonance situation, where the frequency of light and the Bragg and particle-plasmon frequencies are all comparable, we find a complex spatiospectral behavior of the optical near field. The comparison with calculations based on a scattering-matrix approach reveals that the near-field data are dominated by the transverse component of the magnetic field, whereas the far-field spectra are known to be mainly determined by the transverse component of the electric field.

ACKNOWLEDGMENTS

We acknowledge support by the Center for Functional Nanostructures (CFN) of the Deutsche Forschungsgemeinschaft (DFG) within Project Nos. A1.2 and A1.5. The research of K.B. is further supported by DFG Project No. Bu 1107/2-3 (Emmy-Noether program), that of M.W. by Project No. DFG-We 1497/9-1. We thank Philip Chak for his help with the numerical simulations and H. Giessen for discussions.

[1] U. Kreibig and M. Vollmer, *Optical Properties of Metal Clusters* (Springer, Berlin, 1995).
[2] E. Yablonovitch, Phys. Rev. Lett. **58**, 2059 (1987).
[3] S. John, Phys. Rev. Lett. **58**, 2486 (1987).
[4] M. Hübner, J. Kuhl, T. Stroucken, A. Knorr, S. W. Koch, R. Hey, and K. Ploog, Phys. Rev. Lett. **76**, 4199 (1996).
[5] K. C. Huang, P. Bienstman, J. D. Joannopoulos, K. A. Nelson, and S. Fan, Phys. Rev. Lett. **90**, 196402 (2003).
[6] A. Rung and C. G. Ribbing, Phys. Rev. Lett. **92**, 123901 (2004).
[7] B. Lamprecht, G. Schider, R. T. Lechner, H. Ditlbacher, J. R. Krenn, A. Leitner, and F. R. Aussenegg, Phys. Rev. Lett. **84**, 4721 (2000).
[8] S. Linden, J. Kuhl, and H. Giessen, Phys. Rev. Lett. **86**, 4688 (2001).
[9] A. Christ, S. G. Tikhodeev, N. A. Gippius, J. Kuhl, and H. Giessen, Phys. Rev. Lett. **91**, 183901 (2003).
[10] A. Christ, T. Zentgraf, J. Kuhl, S. G. Tikhodeev, N. A Gippius, and H. Giessen, Phys. Rev. B **70**, 125113 (2004).
[11] S. Mononobe and M. Ohtsu, J. Lightwave Technol. **14**, 2231 (1996).
[12] T. Saiki and K. Matsuda, Appl. Phys. Lett. **74**, 2773 (1999).
[13] C. Chicanne, T. David, R. Quidant, J. C. Weeber, Y. Lacroute, E. Bourillot, A. Dereux, G. Colas des Francs, and C. Girard, Phys. Rev. Lett. **88**, 097402 (2002).
[14] W. R. Holland and D. G. Hall, Phys. Rev. Lett. **52**, 1041 (1984).
[15] H. A. Bethe, Phys. Rev. **66**, 163 (1944).
[16] C. J. Bouwkamp, Philips Res. Rep. **5**, 321 (1950).
[17] D. M. Whittaker and I. S. Culshaw, Phys. Rev. B **60**, 2610 (1999).
[18] L. Li, J. Opt. Soc. Am. A **13**, 1870 (1996).
[19] K. Busch, M. Diem, M. Frank, A. Garcia-Martin, F. Hagmann, D. Hermann, S. Mingaleev, S. Pereira, M. Schillinger, and L. Tkeshelashvili, *Photonic Crystals—Advances in Design, Fabrication, and Characterization* (VCH-Wiley, New York, 2004), Chap. 1.
[20] P. B. Johnson and R. W. Christy, Phys. Rev. B **6**, 4370 (1972).